NANO LETTERS

pubs.acs.org/NanoLett Letter

Superradiant Electron Energy Loss Spectroscopy

Ron Ruimy,[†] Alexey Gorlach,[†] Gefen Baranes, and Ido Kaminer*

Cite This: https://doi.org/10.1021/acs.nanolett.2c03396 Read Online

ACCESS | Metrics & More | Article Recommendations | Supporting Information

ABSTRACT: We analyze the interaction between a free electron and an ensemble of identical optical emitters. The mutual coherence and correlations between the emitters can enhance the interaction with each electron and become imprinted on its energy spectrum. We present schemes by which such collective interactions can be realized. As a possible application, we investigate free-electron interactions with superradiant systems, showing how electrons can probe the ultrafast population dynamics of superradiance.

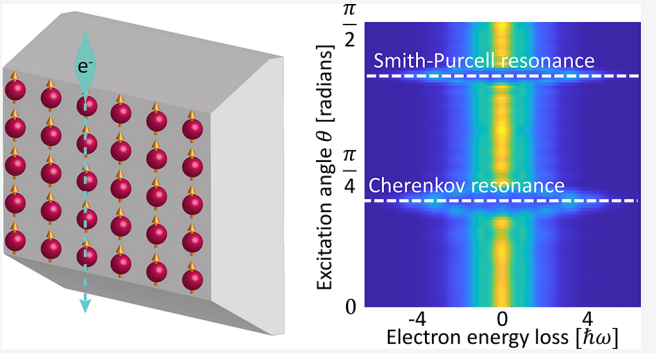

KEYWORDS: *superradiance, free electrons, electron energy loss spectroscopy (EELS), ultrafast transmission electron microscopy (UTEM), quantum coherence, quantum dots*

Electron microscopy and spectroscopy are powerful analytical tools for extracting information about quantum emitters, such as atoms, molecules, vacancy centers, and quantum dots.[1] Specifically, electron-based approaches such as cathodoluminescence[1] and electron energy-loss spectroscopy (EELS)[1] can probe excitation energies, atomic bandgaps, local density of photonic states, and recently even observe phononic-phenomena such as vibrational modes in molecules.[2] In all these examples, free-electron probe techniques can provide very high spatial and energy resolutions.

An emerging field of electron microscopy and spectroscopy is *imaging quantum coherence* of bound electron systems[3−9] and even of light.[10−12] Much theoretical effort in recent years[3−5,13] investigated the coherent interaction between free electrons and discrete quantum systems with energy gap and transitions in the optical range. Such interactions have been proposed as a mean to measure strong-coupling physics with deep-subwavelength resolution,[14] extract the coherent quantum states of quantum emitters,[4,5] generate entanglement between them,[5] and even control their quantum state.[3] A key element necessary for these capabilities is the coherent modulation of the free-electron wave function in the time domain, through photon-induced nearfield electron microscopy (PINEM).[15−25] Such modulated electrons can undergo a coherent resonant interaction with a quantum emitter in a process also called free-electron-bound-electron resonant interaction (FEBERI)[3,4,8,9] or quantum klystron in microwave frequencies.[26] So far, due to the intrinsically weak coupling between free electrons and bound electrons,[4,13] experimental realizations of these phenomena have remained beyond reach.

High densities of emitters hold importance for applications,[27−29] such as semiconductor quantum dot devices for quantum science and technology.[30−32] High emitter densities are a fundamental aspect of certain light−matter interactions, such as superradiance[33−36] and superfluorescence.[37,38] Similarly, the existence of multiple emitters interacting with each other is fundamental for quantum information and computation problems,[39] especially ones that involve collective phenomena and correlations between emitters. These kinds of correlations typically occur at the nanometer scale, making it particularly challenging to probe them with optical techniques, due to the diffraction limit. Those considerations motivate our proposal to use free electrons to probe high-density ensembles of emitters, toward the investigation of many-body quantum physics using free-electron probes. However, so far, the coherent interaction between free electrons and ensembles of quantum systems has yet to be described.

Here, we analyze the coherent interaction between free electrons and an ensemble of identical optical emitters (Figure 1). The electron interaction can be sensitive to the many-body nature of such an ensemble of emitters, strongly enhanced by multiemitter correlations and mutual coherence. We examine these enhanced interactions for the exemplary case of

Received: August 28, 2022
Revised: January 16, 2023

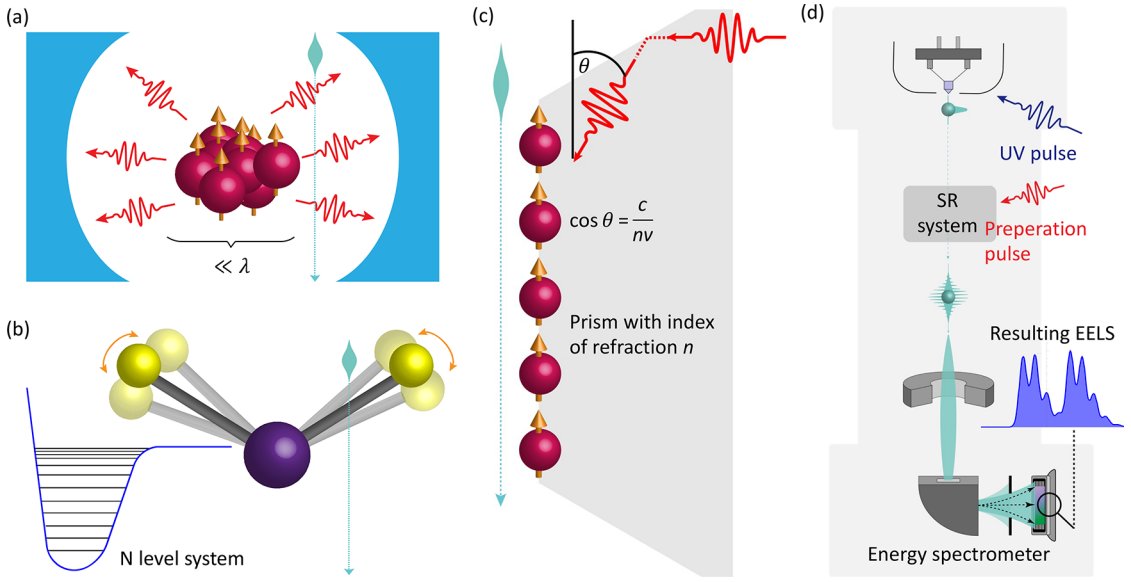

Figure 1. Superradiant electron energy loss spectroscopy (EELS): Systems containing multiemitter correlations that can be investigated using EELS. (a) The high density of emitters confined in a small volume compared to the emitted light wavelength can interact superradiantly. (b) Vibrational modes in molecules are often described by anharmonic oscillators, creating effective N-level systems that mimic superradiant phenomena. (c) Identical quantum emitters arranged along a surface can be synchronized to behave superradiantly even when they are relatively far apart, using their joint interaction with a single electron that correlates between them. We propose such a scenario in a grazing-angle configuration[23] and find that it is governed by a Cherenkov-type phase-matching condition. (d) Superradiant EELS can be realized in an ultrafast transmission electron microscope. A pump laser pulse prepares the state of the initial superradiant system, which then interacts with the electron at a delay depicted by a probe pulse. We can extract the state of the superradiant system and its ultrafast dynamics from the EELS measurement.

superradiant dynamic,[33,34] extracting the entire population statistics of the superradiant states using the electrons. These prospects rely on a key realization: that the multiemitter correlations that enable superradiance also *enhance their interaction with each free electron*. Our work contributes to currents efforts toward the investigation of general many-body quantum phenomena using electrons, aiming to achieve simultaneous subnanometer and femtosecond resolution using experimental setups such as ultrafast transmission electron microscopy (UTEM) (Figure 1d).[14,20−22,40]

We model each emitter as a general multilevel system that is small enough to be treated in the dipole approximation. The emitters are coupled to the near-field of the free electron through dipole interaction. The interaction between the emitters is neglected, which is justified when the distance between neighboring emitters is large enough (larger than 5 nm for our characteristic values) or when the interaction is rapid enough to occur before the characteristic decoherence time T_2^* of interemitters interaction. See SI section I for further discussion of the limiting distance between emitters and SI section III for the effects of T_2^*. We calculate the electron−emitters interaction scattering matrix. The ith emitter is located at position z_i with impact parameter $r_\perp^i$. Each emitter's energy states can be denoted as $|p^i\rangle$, and the energy separation between the states is denoted as $\hbar\omega_i^{pq}$. Assuming paraxiality and weak interaction strength with each individual emitter, the coupling strength between an electron and an emitter is (see SI section I for a discussion on the approximations and their relevance for experiments):

$$g_i^{pq} = \left(\frac{e d_{\perp,pq}^i \omega_i^{pq} K_1\left(\frac{\omega_i^{pq} r_\perp^i}{\gamma v}\right)}{2\pi\varepsilon_0 \gamma \hbar v^2} + \frac{e d_{z,pq}^i \omega_i^{pq} K_0\left(\frac{\omega_i^{pq} r_\perp^i}{\gamma v}\right)}{2\pi\varepsilon_0 \gamma^2 \hbar v^2} \right) e^{-i\omega_i^{pq} z_i / v} \tag{1}$$

Here, v is the average velocity of the electron wavepacket; $d_{pq}^i = \langle p^i | e\mathbf{r} | q^i \rangle$; the vacuum permittivity is ε_0; the Lorentz factor is γ; and $K_0(x)$ and $K_1(x)$ are modified Bessel functions of the second kind. Note that the electron's velocity v play few crucial roles: (1) The coupling depends strongly on the electron's velocity and scales as $\sim 1/v$ over the relevant parameters range. Generally, slower electrons are preferred as long as the other conditions are satisfied. (2) The electron velocity affects the phase of the coupling due to the term $\exp(-i\omega_i^{pq} z_i / v)$. This term will define the phase-matching conditions for extended systems that will contribute the enhanced interaction as will be discussed below. (3) Other parameters in electron microscopy scale favorably for higher electron velocities: The spatial resolution increases, although nanometric resolution is possible for a wide range of electron energies (generally above several tens of keV). Moreover, higher electron energies also enable to keep the beam collimated for a longer distance, which is important for the grazing-angle interaction. Still, in certain cases lower electron velocities are preferred, for example for a stronger coupling strength with confined systems (i.e., when multiple emitters are confined in a volume smaller than the wavelength of the emitted light).

The scattering matrix is given by

$$\mathbb{S} = e^{i \sum_{i,p,q} g_i^{pq} t_i^{pq} b_i^{pq}} \tag{2}$$

where the operators b_i^{pq} are the momentum translation operators[41] with translation of $-\hbar\omega_i^{pq}/v$ defined as $e^{i\omega_i^{pq} / vz}$. The operators t_i^{pq} are the emitters' transition operators $|p_i\rangle\langle q_i|$.

https://doi.org/10.1021/acs.nanolett.2c03396
Nano Lett. XXXX, XXX, XXX−XXX

The Hilbert space of the emitters is hard to analyze because of its size, which is generally $K^N \times K^N$, where N is the number of emitters and K is the number of energy levels in each emitter.

Note that although the bound-electronic system are emitters, the emission time-scale is much longer than the free-electron interaction time, and thus, we can neglect the electron interaction with the emitted radiation. We assume that the emitters radiate spontaneously after their interaction with the free electron.

Eq 2 is completely general; however, for the purpose of this manuscript, we are interested in limited case that capture some of the key phenomena of electron interactions. We assume that all the emitters are identical in terms of transition dipoles and energy levels, differing only in their location on the z axis, creating an effective 1D structure (Figure 1c). Furthermore, we ignore all energy states except the ground state and some excited state with energy separation $\hbar\omega_0$, making the emitters effective two-level systems. This assumption is justified typically when there is one transition dipole moment more dominant than the rest, and when the excitation of the emitter is done with a narrow-band pulse making the population of the other energetic states initially negligible. Furthermore, since this manuscript focuses on resonances arising from the phase matching between an electron and a specific transition, this transition becomes dominant compared to the other transitions (especially in the case of many emitters). In this case, the scattering matrix can be simplified to

$$\mathbb{S} = e^{i(gS_+ b + g^* S_- b^\dagger)} \tag{3}$$

g is the coupling strength defined in eq 1, and b is the momentum translation operator for the free electron with translation $-\hbar\omega_0/v$ and $S_\pm = \sum_i \sigma_\pm^i e^{\mp i\omega_0 z_i/v}$ where $\sigma_\pm$ are Pauli matrices. These super operators define a superradiant ladder that can be constructed by acting with these operators on the ground state $|m\rangle = \frac{1}{\sqrt{\binom{N}{m}}} S_+^m |gg...g\rangle$. The state $|m\rangle$ is a superposition state of all the different permutations of states with a total of m excited emitters, with an additional phase factor that depends on the excited emitters position. Without these phase factors, the states correspond to the maximally symmetric (maximal "cooperation" number[33]) Dicke states, which are used in the common description of superradiance. Notice that we index the states from 0 to N while in Dicke paper they are indexed from $-N/2$ to $N/2$. The scattering matrix is closed in the sub-Hilbert space of this superradiant ladder. If the initial state of the emitters is in this sub-Hilbert space, then the scattering matrix is reduced to be $(N+1) \times (N+1)$ for the emitters. A detailed derivation is presented in SI section I.

To understand the in what sense this ladder is superradiant, we write the $S_\pm$ operators in the interaction picture (with respect to the emitters free Hamiltonian):

$$S_\pm^I = \sum_i \sigma_\pm^i e^{\pm i\omega_0 (t - \frac{z_i}{v})} \tag{4}$$

The electron arrives to the emitter located at z_i at time z_i/v and, thus, experiences a delayed interaction with the different emitters. From the reference frame of the electron, these operators are Dicke superradiance ladder operators of a sub-Hilbert space of maximally symmetric Dicke states that are phase shifted according to the corresponding delays. If the emitters are initially at the ground state, the electron excitation keeps them inside this symmetric (superradiant) sub-Hilbert space spanned by the operators $S_\pm$. Also, if the emitters are pre-excited to satisfy phase-matching condition with the electron, the interaction keeps them inside this superradiant sub-Hilbert space. From the perspective of the electron, all the transition dipoles add up constructively as is the typical case in Dicke superradiance,[33] resulting in an effective dipole with size $N{\cdot}d$. Note that the operators in eq 4 reproduce conventional Dicke superradiance[33,34] when the emitters are located close enough to each other, typically within a single wavelength[34] (Figure 1a). The same mathematical framework we develop also applies to equally spaced N-level systems such as the anharmonic oscillator modeling of vibrational states in molecules[42] (Figure 1b).

The elements of the scattering matrix can be found analytically and are given by

$$\begin{aligned} s_{nm} &= \langle n|S|m\rangle \\ &= b^{n-m}(\cos|g|)^N (i\tan|g|)^{n-m} \\ &\quad \times \sqrt{m!n!(N-n)!(N-m)!} \sum_{k=0}^{m} \frac{(-1)^k (\tan|g|)^{2k}}{k!(m-k)!(n-m+k)!(N-n-k)!} \end{aligned} \tag{5}$$

Here, the momentum translation operator b from eq 3 is used to define $b^{-N} \equiv b^{\dagger N}$. If we assume that $|g| \ll 1$ and additionally $N - m \gg 1$ and $m \gg 1$, meaning that the state is far from the edges of the ladder, then eq 5 can be further simplified (see SI section II):

$$s_{nm} \approx J_{n-m}(2|g|\sqrt{Nm - m^2}) e^{i(n-m)\arg(g)} \tag{6}$$

In this approximation, the scattering matrix approaches that of a coherent interaction between a free electron and light, as in photon-induced nearfield electron microscopy.[18] The similarity arises when the photonic excitation in its quantum harmonic oscillator is far from the ground state, and then it resembles the ladder states far from the edges. The resulting effective coupling equals $g_{\text{eff}} = |g|\sqrt{Nm - m^2}$. Let us consider a coherent control ϕ pulse,[43,44] after which the single two-level system is in superposition with probability $\cos^2(\phi/2)$ to be in the ground state and $\sin^2(\phi/2)$ to be in the excited state. If we imagine for example that the emitters are excited using a coherent control ϕ pulse, then the states are narrowly distributed around $m = \sin^2\left(\frac{\phi}{2}\right)N$, and we can approximate the effective coupling as

$$g_{\text{eff}} = \frac{\sin(\phi)}{2} Ng \tag{7}$$

The most important result here is that g_{eff} scales like N and not like $\sqrt{N}$ as expected from noncorrelated interactions. This enchantment is due to the mutual quantum coherence between the emitters and is analogous yet complementary to the effect of free-electron-bound-electron resonant interaction:[3] There, each electron's wave function is bunched periodically so its constituents all see the same phase of a single oscillating emitter, whereas here, an ensemble of emitters are all organized so their oscillating phase is seen as constant by a single moving electron (independent of its wave function shape, even in the vicinity of electron modulation). Both effects give a resonant interaction between the emitters and the

https://doi.org/10.1021/acs.nanolett.2c03396
Nano Lett. XXXX, XXX, XXX−XXX

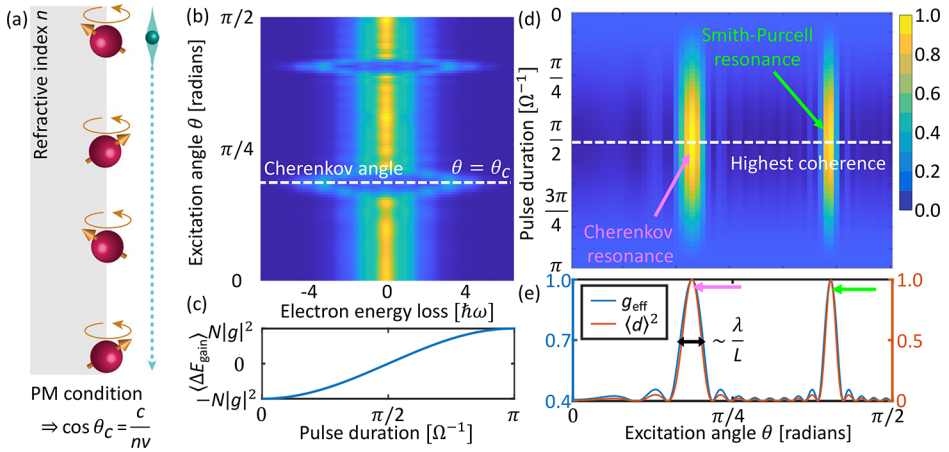

Figure 2. Phase-matched interaction between multiple emitters distributed over an extended area and a single electron that mediates their collective interaction. (a) System schematic. Emitters excited by a laser with its wavefront tilted by an angle θ, creating a relative delay between consequent emitters of $\Delta t = \cos\theta\, \Delta z n/c$. A free electron with velocity v interacts with the emitters at a certain phase delay $\Delta t = \Delta z/v$, creating a resonant interaction when the time it takes to pass between consequent emitters matches the delay induced by the laser excitation. The condition for such a resonant interaction is Cherenkov-type ($\cos(\theta_C)n/c = 1/v$). This condition also enables the superradiant EELS phenomenon. (b) EELS as a function of excitation angle by a $\pi/2$ pulse. The strongest interaction is achieved at the Cherenkov angle θ_C, satisfying phase matching between the electron and the emitters. (c) The net energy transfer from the emitters to the electron as a function of the excitation pulse duration. (d) The effective coupling g_{eff} as a function of the excitation pulse duration and angle. The Smith−Purcell-type resonances arise from the periodicity in the positions of the emitters (taken here to be 1 μm). Similar Smith−Purcell peaks are predicted in ref 53 for classical electrons and emitters in the ground state, while our work considers an extended electron wave function and initially excited emitters. If the emitters are placed in random locations, the Cherenkov-type resonance remains, but the Smith−Purcell-type resonances vanish. (e) The effective coupling for a $\pi/2$ pulse, in comparison with the expectation value of the dipole as seen by the electron, both normalized to their respective maximal value. The width of the Cherenkov resonance is robust to disorder in the position of emitters and depends on the ratio between the emitters' radiation wavelength λ and the total interaction length L (see SI section III). All plots are normalized by peak value. The parameters for these plots are $v = 0.7c$, $N = 10$, $|g| = 0.5$.

electrons but from a complementary physical origin. Throughout the manuscript, we consider the electrons as monoenergetic. This approximation holds when the electron energy spread is smaller than the energy $\hbar\omega$ of the optical excitation with which the electron interacts, a common situation in electron microscopes. Considering a monoenergetic electron is equivalent to having the electron temporal spread much longer than the optical cycle of the emitters' radiation.

Another consequence of this complementarity is that whereas free electrons can induce Rabi oscillations on a single emitter in ref 3, in our work the ensemble of emitters induce Rabi oscillations on a single electron as can be shown through eq 6.[15−18] Future works could investigate the interplay of these two types of Rabi oscillations when both the electron's and the emitter's mutual coherence are presented simultaneously.

There exist two types of superradiance: Dicke superradiance, where the emitters act as an effective big dipole, and free-electron superradiance, where the electrons act as an effective big charge (as used in klystrons,[45] synchrotrons,[46,47] and free-electron lasers (FELs)[47,48]). This work focuses on the first type, and thus, our predictions apply even with just a single electron. Nevertheless, we note that these two types of superradiance can happen simultaneously, resulting in a double enhancement of EELS, and of the resulting cathodoluminescence signal.[49] The EELS cross-section is typically proportional to $(d\cdot e)^2$, with d being the dipole strength and e being the electron charge. The superradiance of the emitters and/or electrons enhance the cross-section by scaling $d \to N_a d$ and/or $e \to N_e e$ with $N_{a/e}$ being the number of emitters and electrons, respectively. Note that in this work, we demonstrate superradiant enhancement of the electron-emitters' interaction and show how the free electrons can interrogate the superradiative emission process of the emitters. The superradiant state of the emitters can be excited via any conventional interaction mechanism that implements coherent control, e.g., a laser pulse or coherently modulated free electrons.[3,8,9,49]

For an ensemble of excited emitters to satisfy a phase matched interaction with the electron, they need to be excited such that they remain inside the superradiant sub-Hilbert space following their (delayed) interactions with the electron. This implies that the relative phase between emitters separated by Δz should be $\omega_0\, \Delta z/v$. Since $v < c$, such a relative phase cannot be achieved by a free-space laser excitation, and so a material with an index of refraction n can be utilized as illustrated in Figure 1c. For a laser excitation propagating through such a material at angle θ, the phase-matching condition translates to the following condition on the angle:

$$\cos\theta_C = \frac{c}{nv} \tag{8}$$

This is exactly the Cherenkov condition[50,51] for phase matching between light and an electron. However, unlike all previous works in the field, here the phase matching is between the quantum emitters and an electron.

Previous works that referred to superradiant effects in free-electron radiation (e.g., klystron, synchrotron, free-electron lasers[52]) generally considered other type of superradiance—free-electron superradiance—arising from the number of free-electrons. Here, we access a different phenomenon—Dicke superradiance—arising from the quantum nature of the emitters and their correlated excitation. The first step toward Dicke superradiance excited by free electrons has been

https://doi.org/10.1021/acs.nanolett.2c03396
Nano Lett. XXXX, XXX, XXX−XXX

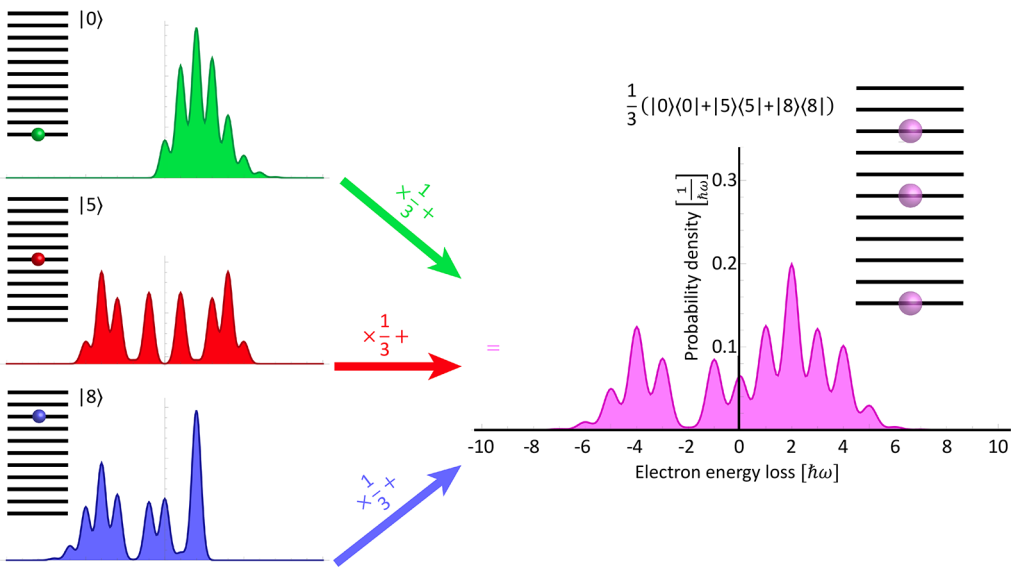

Figure 3. Extracting the population of the superradiant states from EELS measurements. The EELS is found to be an incoherent weighted sum of the corresponding electron spectra of the different states on the ladder. Therefore, the population can be inferred by decomposing the spectrum according to eq 12. The parameters are taken to be the same as in Figure 2.

suggested in ref 53; however, the analysis there considered emitters in their ground state and a classical point-particle description of the electrons. Following recent advances in the field, we now know that since we consider emitters in the optical range, the wave nature of the electron is necessary for a full description of their interaction. In this case, the superradiant interaction arises from premodulated mutual coherence between the emitters (coming from a coherent excitation such as by a laser pulse), rather than from the electron excitation. Our work constitutes the first analysis of the quantum mechanical interaction between a Dicke-type superradiance system and a free electron. Studying such an interaction is motivated by recent works,[4,8,9] in which a dense ensemble of emitters confined within a small volume was treated as a larger dipole, referred to as a superqubit.[8,9]

To realize such an interaction, we imagine a prism, such as in Figure 1c, and multiple emitters such as quantum-dots[30,32] or perovskites[54−56] positioned on the surface of the prism. The laser excites the emitters with an angle matching the Cherenkov condition for an electron impinging at a grazing angle.[23] The EELS of an electron arriving *during* the laser excitation is expected to be dominated by the direct electron-laser interaction (enhanced by the same phase-matching condition[23]), rather than by the electron-emitters interaction. The signature of electron-emitters interaction should appear for an electron arriving after the laser excitation is over, and before the emitters lose the relative phase between them, quantified by the ensemble decoherence time T_2^*. Arrays of QDs can provide sufficient T_2^*: on the picoseconds scale even in room temperatures,[57,58] which is long enough for typical interaction durations of electrons in grazing-angle configurations (hundreds of femtoseconds).[23] Therefore, the necessary conditions to observe the electron-emitters phase-matched interaction exist using readily available materials and experimental configurations.

In Figure 2, we look at the electron energy spectra postinteraction for the initially monoenergetic electron ($|\psi_e\rangle = |E_0\rangle$) with multiple emitters after a $\pi/2$ pulse arriving at different angles. A $\pi/2$ pulse is considered to maximize the emitters' coherence (and hence, the effective coupling, see eq 7). Figure 2b shows that when the phase-matching condition is satisfied, the postinteraction EELS becomes much wider, indicating a stronger interaction. We note that although the coupling is enhanced, as long as the electron wave function is not modulated, this enhancement does not contribute to the net energy transfer between the electron and the emitters. The only net energy transfer will be significantly smaller, arising from spontaneous emission and scaling as $|g|^2$. This effect can be calculated by incoherently summing up the net energy transfer to an individual emitter (as calculated in ref 4) and is shown in Figure 2c. To quantify the enchantment in the coupling, we define the effective coupling constant of one interaction according to

$$g_{\text{eff}} \equiv \frac{\sigma_{\text{EELS}}}{\sqrt{2}\,\hbar\omega_0} \tag{9}$$

where σ_{EELS} is the standard deviation of the resulting energy distribution. This definition is consistent with the analogy to photoinduced nearfield electron microscopy in eq 6. In Figure 2d, we plot the normalized effective coupling, confirming that the maximum coupling is achieved in the phase-matching condition, with a $\pi/2$ excitation.

Figure 2d, e shows oscillations in the effective coupling that we attribute to higher-order phase-matching arising from Smith−Purcell-like conditions (modified by the material's refractive index) due to the periodicity of the emitters' positions.[59,60] To understand this effect, we write the dipole expectation value as seen by the moving electron (see Figure 2e):

$$|\langle d(\theta)\rangle|^2 = d_0^2 \left| \sum_i e^{i\omega_0 z_i \left(\frac{n\cos\theta}{c} - \frac{1}{v}\right)} \right|^2 \tag{10}$$

To find the resonant excitation angles marked in Figure 2d, e, we require for the arguments of the exponents in eq 10 to be multiples of 2π, which exactly yields a hybrid Cherenkov−

https://doi.org/10.1021/acs.nanolett.2c03396
Nano Lett. XXXX, XXX, XXX−XXX

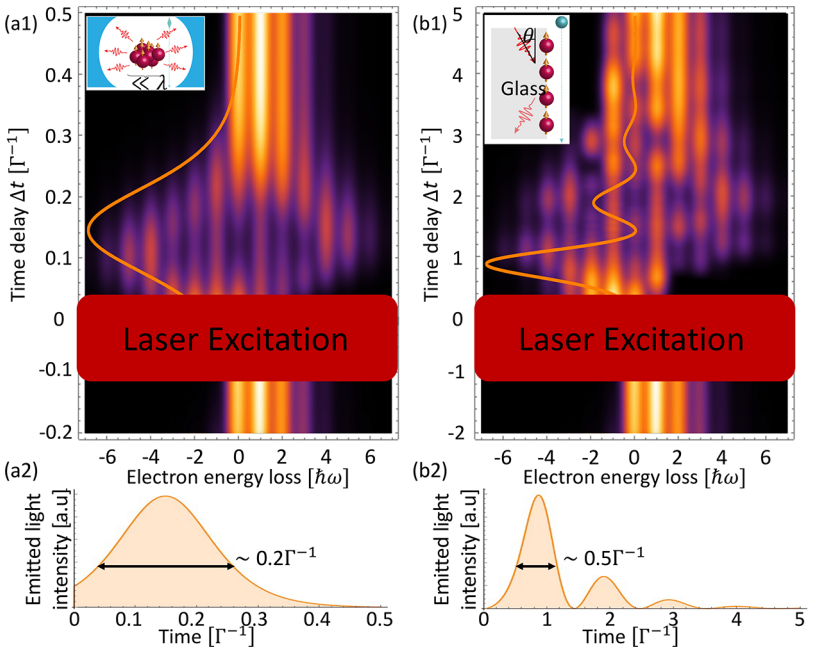

Figure 4. Extracting information about the superradiance dynamics from EELS. The emitters are initiated at the fully excited states using a (π-pulse) laser excitation (marked on the panels). Panels (a1) and (b1) show electron energy loss after the interaction of free electrons with the system of emitters at different delays Δt between the excitation and the electron interaction. For negative and large positive delays, the system of emitters is in the ground state, which leads only to loss of electron energy in the interaction (3−4 energy loss peaks for the considered parameters). Panel (a1) describes a dense-ensemble situation as in Figure 1a, and panel (b1) describes a grazing-angle configuration as in Figure 1c. A free electron measures their state as a function of the time delay, showing the population relaxation during the superradiant emission. The delay is shown in units Γ^{-1}, where Γ is the spontaneous emission rate of a single emitter. We emphasize that the vertical axis in (a1) and (b1) are different. The duration of the pulse is longer in (b1) than in (a1) since the sample is much longer and the propagation effects take place.[34] The EELS at each time delay enables extracting the emitters' population on the superradiant ladder according to eq 12. Panels (a2) and (b2) present the corresponding time-dependent intensity plots. Superradiant ringing,[34] which is the oscillations of the emitted light intensity with time, occurs for the long sample (b2) due to propagation effects and makes the duration of light emission much longer than for the small sample in (a2). The parameters for these plots are $v = 0.7c$, $N = 30$, $|g| = 0.2$.

Smith−Purcell condition as described in ref 61 for the inverse effect (i.e., for light emission by the emitters rather than for resonant electron interaction with pre-excited emitters). The periodicity in the locations of the emitters yields constructive interference in the interaction with the electron at these additional excitation angles besides the Cherenkov angle, according to the modified Smith−Purcell formula:

$$\cos\theta_K = \frac{c}{nv} - \frac{2\pi c}{\Delta z n \omega_0} K \tag{11}$$

Here, Δ_z is the spacing between emitters, and K is the resonance index, where $K = 0$ corresponds to the Cherenkov resonance.

When the state of the emitters is part of the superradiant ladder, the entire population of the emitters is encoded on the free electron's postinteraction energy spectrum. This allows us to reconstruct the quantum state of the emitters using EELS. To show this, consider a general superradiant state of the form $\rho_a = \sum \rho_{mn} |m\rangle\langle n|$ interacting with a free electron. The resulting EELS for the initially monoenergetic electron $|\psi_e\rangle = |E_0\rangle$ contain the probability of the electron to lose k quanta of energy:

$$P_{-k} = \sum_m d_{km} \rho_{mm},$$
$$d_{km} = (\cos|g|)^N (i \tan|g|)^{k-m} \sqrt{m!k!(N-k)!(N-m)!} \sum_{n=0}^{m} \frac{(-1)^n (\tan|g|)^{2n}}{n!(m-n)!(k-m+n)!(N-k-n)!} \tag{12}$$

Then, the population statistics can be constructed from the energy spectrum by inverting the matrix d_{km}. The reconstruction process will go as follows: the emitters are excited to a state with a certain population statistics using a reproducable experiment, such as exciting the emitters with a laser pulse with a given intensity and duration and then waiting some fixed amount of time delay before interacting with the electron. The electron interaction takes place within a femtosecond time scale such that we can assume that the emitters' state is frozen during the interaction. After repeating the experiment many times, the population statistics of the emitters' will be encoded on the electron energy spectrum according to eq 12, as illustrated in Figure 3 for some exemplary superposition (coherent or incoherent) of some superradiant states. We can then reconstruct the statistics ρ_{mm} of the superradiant system at a given time delay and measure the population dynamics $\rho_{mm}^{(t)}$ of the emitter's system during the emission by varying the time delay.

For a more general initial electron state $|\psi_e\rangle = \sum g_k |E_0 + k\hbar\omega_0\rangle$ that can be generated using coherent

https://doi.org/10.1021/acs.nanolett.2c03396
Nano Lett. XXXX, XXX, XXX−XXX

modulation of the free-electron wavepacket,[22,23] the final energy spectra will also include decodable information about the off-diagonal elements ρ_{mn} $(m \neq n)$ of the superradiant state (similar to that in ref 4). Consequently, each term $|E_0 + k\hbar\omega_o\rangle$ in the initial electron superposition state, will allow to extract information about the off-diagonal elements $\rho_{m,m+k}$. The detailed theory of the reconstruction of the off-diagonal elements with shaped electrons is left for the future work.

The dynamics of Dicke Superradiance[33,34] includes a rapid relaxation of the identical emitters to their ground state, accompanied by emission of a short and intense pulse of light. This phenomenon results from the coherence and indistinguishability between the emitters, keeping them in the superradiant ladder during their relaxation dynamics. Many of the open questions about the process of Dicke superradiance relate to the population statistics of the emitters in the superradiant ladders, and the internal correlations between different ladder states. Typical measurements of superradiance rely on the emitted pulse intensity, which only reveals the mean-field dynamic of the emitters' population.[34−36] However, as shown by Bonifacio et al.,[35,36] much interesting information lies beyond the mean-field approximation: for example, relating higher order correlations of the emitted light to correlations in the ladder states. We expect the full quantum state of superradiant light to depend on the correlations between the different superradiant states, and the photon statistics (and therefore the Mandel Q parameter[62]) to depends on the population statistics. Figure 4a presents our proposal for extracting the population statistics of the emitters during superradiance using their interaction with a free electron.

Figure 4 exemplifies EELS measurements for extracting the transient population statistics of the emitters. For each electron measurement, the emitters are excited by a laser pulse at time $t = 0$ and interact with an electron at a later time $t = \Delta t$. To get enough statistics for the electron energy spectrum, such a pump−probe scheme is repeated for each fixed delay Δt, to accumulate signal (the emitters are re-excited to the same state in each cycle). Then, these measurements are repeated for different time delays to reconstruct the population dynamic. Such a scheme requires pulses of light with stable intensity and duration, as is typical in coherent control pump−probe experiments (such as[58]). Such a scheme requires stability in pulse of light between repetitions of the experiments (same intensity and duration), which is the typical procedure in coherent control pump−probe experiments (such as ref 58). We emphasize that, according to eq 12, the EELS is not sensitive to the phase of excitation pulse hence the light excitation should not have the same phase for each repetition but only have the same intensity and duration. The ϕ-pulse can be prepared experimentally as discussed in ref 44 for an arbitrary optical ϕ-pulse. Such coherent control abilities have been recently demonstrated even in room temperature high-density quantum dot systems such as in ref 58.

The emission intensity envelope is encoded on the electron's energy spectrum, together with the entire population statistics as shown in Figure 4. Using the reconstruction scheme detailed above, the emitters' state can be reconstructed (for times shorter than decoherence T_2^* so their state remains in the sub-Hilbert space). Figure 4b exemplifies this scheme for long-sample superradiance,[34] using the truncated-Wigner approximation[63] to calculate the superradiant dynamic (see SI section III). The phase-matching condition on the excitation laser provides the emitters with a phase relation enabling superradiance and decay inside the superradiant ladder. The long-sample nature gives rise to a characteristic fluctuating intensity pattern. To the best of our knowledge, solving the population dynamic in such a system beyond the mean-field approximation is a difficult problem without a known analytical solution;[34,37] this motivates an experimental investigation of the scheme we present here.

Looking at the grater field of EELS gives our theory a wider context: as an instance of **EELS for out-of-equilibrium systems**, showing the importance of mutual coherence in matter for interactions with free electrons. This goes beyond the conventional theory of EELS[7] that rely on systems in equilibrium and on linear response theory.[64−66] Our work, thus, contributes to our ongoing efforts toward a general understanding of out-of-equilibrium EELS, which was so far only investigated for electron interaction with a single quantum emitter.[4] Advances in ultrafast electron microscopy[14−23,40] now make it possible to investigate this new area experimentally.

So far, the coherence of quantum emitters was seen as important only for interactions with coherently modulated electrons.[3−6,8,9] Our work shows that when the coherence involves multiple systems, it affects the interaction even with nonmodulated electrons, which opens new paths for experimental observations of such phenomena. Furthermore, coherent interaction of free electrons with bound electron systems[3−9,13] is yet to be observed experimentally due to the intrinsically weak coupling. Our proposal of utilizing an ensemble of identical emitters interacting with a single electron can enhance the interaction significantly, enabling experiments in new complementary systems.

The Dicke superradiance process is typically probed optically by measuring the emitted pulse. However, understanding the superradiant dynamic on small scales, at spatial resolutions beyond the reach of optical methods, remains a great challenge. The electron interaction opens the possibility of using electron pulses to image the dynamics of Dicke superradiance, extracting the intermediate populations on the superradiant ladder with simultaneous high spatial and temporal resolution, as in ultrafast transmission electron microscopy.[14,40]

A realistic system that can demonstrate all the predicted features in an experiment will include high-quality quantum emitters (such as the quantum dots in refs 57 and 58) glued on the surface of a glass prism positioned in a similar configuration to that in ref 23 (Figure 1c). The interaction length of the free electron with the prism can be more than $L = 100\ \mu$m.[23] The distance between neighboring quantum dots can range from 10 nm up to a few microns, which is enough to neglect interactions between emitters (SI section I). We discuss in SI section III the possible effect of disorder in energy, position, orientation, and interaction strength of the emitters, and conclude that the predicted resonances are robust. The variation in emitter energies and other harmful effects for the superradiance can be described by the T_2^* decoherence time. Modern fabrication techniques can achieve long decoherence times on the picoseconds scale even in room temperatures,[57,58] which is longer than the time of interaction (dozens of femtoseconds).[23] Similarly to ref 53, the number of emitters with which each electron can interact coherently is approximated by $vT_2^*/\Delta z$, where Δz is the distance between neighboring emitters. This numbers can range between hundreds to thousands of emitters depending on the specific

https://doi.org/10.1021/acs.nanolett.2c03396
Nano Lett. XXXX, XXX, XXX−XXX

parameters. Considering characteristic values of the electron-emitter coupling $|g| \sim 10^{-3}$,[4] the resonances presented in this work can enhance the effective electron-emitters coupling to be above unity, resulting in a strong interaction well within the detectable range of free electron pump−probe experiments.

To conclude, our work investigated for the first time the coherent interaction between a free electron and an ensemble of emitters. We found resonances in the electron-emitters interaction, facilitated by the mutual coherence between the emitters. Free electrons can be utilized to investigate superradiance over spatial and temporal resolutions that are inaccessible to conventional optical techniques. Besides the enhanced resolution, the electrons provide quantum information regarding the emitters' state, which is inaccessible using conventional measurement techniques in superradiance. Further information on the quantum state of the emitters, such as their off-diagonal coherences,[4,5] can be accessed as well by preshaping the electron before its interaction,[3−5] potentially enabling even stronger superradiant-EELS resonances.

■ ASSOCIATED CONTENT

Supporting Information

The Supporting Information is available free of charge at https://pubs.acs.org/doi/10.1021/acs.nanolett.2c03396.

Detailed derivation of all the results in this manuscript and further discussions on the effects of disorder (PDF)

■ AUTHOR INFORMATION

Corresponding Author

Ido Kaminer − *Solid State Institute and Faculty of Electrical & Computer Engineering, Technion-Israel Institute of Technology, Haifa 32000, Israel;* orcid.org/0000-0003-2691-1892; Email: kaminer@technion.ac.il

Authors

Ron Ruimy − *Solid State Institute and Faculty of Electrical & Computer Engineering, Technion-Israel Institute of Technology, Haifa 32000, Israel*

Alexey Gorlach − *Solid State Institute and Faculty of Electrical & Computer Engineering, Technion-Israel Institute of Technology, Haifa 32000, Israel*

Gefen Baranes − *Solid State Institute and Faculty of Electrical & Computer Engineering, Technion-Israel Institute of Technology, Haifa 32000, Israel;* orcid.org/0000-0002-5920-2972

Complete contact information is available at: https://pubs.acs.org/10.1021/acs.nanolett.2c03396

Author Contributions

†Equal contributors

Notes

The authors declare no competing financial interest.

■ ACKNOWLEDGMENTS

The authors would like to thank Prof. Gadi Eisenstein for sharing with us his expertise in semiconductor quantum dot science and for insightful discussions. This project has received funding from the European Research Council (ERC) Starting Grant No. 851780-NanoEP and the European Union's Horizon 2020 research and innovation program under grant agreement No. 9645919-SMARTelectron.

■ REFERENCES

(1) Polman, A.; et al. Electron-beam spectroscopy for nanophotonics. *Nat. Mater.* **2019**, *18*, 1158.
(2) Krivanek, O.; et al. Vibrational spectroscopy in the electron microscope. *Nature* **2014**, *514*, 209.
(3) Gover, A.; Yariv, A. Free-Electron-Bound-Electron Resonant Interaction. *Phys. Rev. Lett.* **2020**, *124*, 064801.
(4) Ruimy, R.; et al. Toward Atomic-Resolution Quantum Measurements with Coherently Shaped Free Electrons. *Phys. Rev. Lett.* **2021**, *126*, 233403.
(5) Zhao, Z.; et al. Quantum entanglement and modulation enhancement of free-electron-bound-electron interaction. *Phys. Rev. Lett.* **2021**, *126*, 233402.
(6) Pan, Y.; Gover, A. Beyond Fermi's golden rule in free-electron quantum electrodynamics: acceleration/radiation correspondence. *New J. Phys.* **2021**, *23*, 063070.
(7) García De Abajo, F. J. Optical excitations in electron microscopy. *Rev. Mod. Phys.* **2010**, *82*, 209−275.
(8) Zhang, B.; et al. Quantum state interrogation using a preshaped free electron wavefunction. *Phys. Rev. Res.* **2022**, *4*, 033071.
(9) Ran, D.; et al. Coherent excitation of bound electron quantum state with quantum electron wavepackets. *Front. Phys.* **2022**, *10*, 547.
(10) Baranes, G.; et al. Free electron can induce entanglement between photons. *NPJ. Quantum Inf.* **2022**, *8*, 32.
(11) Dahan, R.; et al. Imprinting the quantum statistics of photons on free electrons. *Science.* **2021**, *373*, 6561.
(12) Kfir, O.; et al. Optical coherence transfer mediated by free electrons. *Sci. Adv.* **2021**, *7*, 18.
(13) García de Abajo, F. J.; et al. Complete Excitation of Discrete Quantum Systems by Single Free Electrons. *Phys. Rev. Lett.* **2022**, *129*, 093401.
(14) Karnieli, A.; et al.Probing strongly coupled light-matter interactions using quantum free electrons. *2022 Conference on Lasers and Electro-Optics (CLEO)*, San Jose, CA, USA, 2022.
(15) Barwick, B.; et al. Photon-induced near-field electron microscopy. *Nature* **2009**, *462*, 902.
(16) García De Abajo, F. J.; et al. Multiphoton absorption and emission by interaction of swift electrons with evanescent light fields. *Nano Lett.* **2010**, *10*, 1859.
(17) Park, S. T.; et al. Photon-induced nearfield electron microscopy (PINEM): Theoretical and experimental. *New J. Phys.* **2010**, *12*, 123028.
(18) Feist, A.; et al. Quantum coherent optical phase modulation in an ultrafast transmission electron microscope. *Nature* **2015**, *521*, 200.
(19) Echternkamp, K. E.; et al. Ramsey-type phase control of free-electron beams. *Nat. Phys.* **2016**, *12*, 1000.
(20) Priebe, K. E.; et al. Attosecond electron pulse trains and quantum state reconstruction in ultrafast transmission electron microscopy. *Nat. Photonics.* **2017**, *11*, 793.
(21) Vanacore, G. M.; et al. Attosecond coherent control of free-electron wave functions using semi-infinite light fields. *Nat. Commun.* **2018**, *9*, 2694.
(22) Vanacore, G. M.; et al. Ultrafast generation and control of an electron vortex beam via chiral plasmonic near fields. *Nat. Mater.* **2019**, *18*, 573.
(23) Dahan, R.; et al. Resonant phase-matching between a light wave and a free-electron wavefunction. *Nat. Phys.* **2020**, *16*, 1123.
(24) Reinhardt, O.; Kaminer, I. Theory of Shaping Electron Wavepackets with Light. *ACS Photonics.* **2020**, *7*, 2859.
(25) Yalunin, S. V.; et al. Tailored high-contrast attosecond electron pulses for coherent excitation and scattering. *Phys. Rev. Research.* **2021**, *3*, 032036.
(26) Ratzel, D.; et al. Controlling quantum systems with modulated electron beams. *Phys. Rev. Research.* **2021**, *3*, 023247.
(27) Ledentsov, N. N.; et al. Quantum dot heterostructures: fabrication, properties, lasers. *Semiconductors.* **1998**, *32*, 343−365.
(28) Bimberg, D.; Pohl, U. W. Quantum dots: promises and accomplishments. *Mater. Today.* **2011**, *14* (9), 388−397.

(29) Shen, H.; et al. Visible quantum dot light-emitting diodes with simultaneous high brightness and efficiency. *Nature Photonics.* **2019**, *13*, 192−197.
(30) Banyoudeh, S.; Reithmaier, J. P. High-density 1.54 μm InAs/InGaAlAs/InP (100) based quantum dots with reduced size inhomogeneity. *J. Crystal Growth.* **2015**, *425*, 299−302.
(31) Choi, H.; et al. Ultrafast Rabi flopping and coherent pulse propagation in a quantum cascade laser. *Nature Photonics.* **2010**, *4*, 706−710.
(32) Bayer, M.; Forchel, A. Temperature dependence of the exciton homogeneous linewidth in $In_{0.60}Ga_{0.40}As$/GaAs self-assembled quantum dots. *Phys. Rev. B* **2002**, *65*, 041308.
(33) Dicke, R. H. Coherence in spontaneous radiation processes. *Phys. Rev.* **1954**, *93*, 99.
(34) Gross, M.; Haroche, S. Superradiance: An essay on the theory of collective spontaneous emission. *Phys. Rep.* **1982**, *93*, 301−396.
(35) Bonifacio, R.; et al. Quantum Statistical Theory of Superradiance. I. *Phys. Rev. A* **1971**, *4*, 302.
(36) Bonifacio, R.; et al. Quantum Statistical Theory of Superradiance. II. *Phys. Rev. A* **1971**, *4*, 854.
(37) Bonifacio, R.; et al. Cooperative radiation processes in two-level systems: Superfluorescence. *Phys. Rev. A* **1975**, *11*, 1507.
(38) Rainò, G.; et al. Superfluorescence from lead halide perovskite quantum dot superlattices. *Nature.* **2018**, *563*, 671−675.
(39) Nielsen, M. A.; Chuang, I.*Quantum Computation and Quantum Information*; Cambridge University Press: New York, USA, 2002.
(40) Wang, K.; et al. Coherent interaction between free electrons and a photonic cavity. *Nature* **2020**, *582*, 50−54.
(41) Rivera, N.; Kaminer, I. Light-matter interactions with photonic quasiparticles. *Nat. Rev. Phys.* **2020**, *2*, 538−561.
(42) Morse, P. M. Diatomic Molecules According to the Wave Mehcanics. II. Vibrational Levels. *Phys. Rev. A* **1929**, *34*, 57.
(43) Garrison, J.; Chiao, R.*Quantum Optics*; Oxford University Press, 2008.
(44) Ramsay, A. J. A review of the coherent optical control of the exciton and spin states of semiconductor quantum dots. *Semicond. Sci. Technol.* **2010**, *25*, 103001.
(45) Gilmour, A. S.*Klystrons, Traveling Wave Tubes, Magnetrons, Crossed-Field Amplifiers, and Gyrotrons*; Artech House, 2011.
(46) Nodvick, J. S.; Saxon, D. S. Suppression of coherent radiation by electrons in a synchrotron. *Phys. Rev.* **1954**, *96*, 180.
(47) Gover, A.; et al. Time and frequency domain analysis of superradiant coherent synchrotron radiation in a waveguide free-electron laser. *Phys. Rev. Lett.* **1994**, *72*, 1192.
(48) Pellegrini, C.; et al. The physics of x-ray free-electron lasers. *Rev. Mod. Phys.* **2016**, *88*, 15006.
(49) Reinhardt, O. Superradiant Chatodeluminescence. *Conference on Lasers and Electro-Optics* **2021**, No. FW2Q.6, DOI: 10.1364/CLEO_QELS.2021.FW2Q.6.
(50) Cherenkov, P. A. Visible Emission of Clean Liquids by Action of γ radiation. *Dokl. Akas. Nauk SSSR.* **1934**, *2*, 541.
(51) Tamm, I. E.; Frank, I. M. Coherent In-Medium Fast-Electron Radiation. *Dokl. Akas. Nauk SSSR.* **1937**, *14*, 109.
(52) Gover, A. Superradiant and stimulated-superradiant emission in prebunched electron-beam, radiators. I. Formulation. *Phys. Rev. ST Accel. Beams* **2005**, *8*, 030701.
(53) Halperin, A.; et al. Electron-beam-induced super-radiant emission from a grating. *Phys. Rev. A* **1994**, *50*, 3316.
(54) Kumar Jena, A.; et al. Halide Perovskite Photovoltaics: Background, Status, and Future. *Chem. Rev.* **2019**, *119* (5), 3036−3103.
(55) Akkerman, Q. A.; et al. Genesis, challenges and opportunities for colloidal lead halide perovskite nanocrystals. *Nat. Mater.* **2018**, *17*, 394−405.
(56) Sutherland, B. R.; Sargent, E. H. Perovskite photonic sources. *Nat. Photonics* **2016**, *10*, 295−302.
(57) Khanonkin, I.; et al. Ramsey fringes in room-temperature quantum-dot semiconductor optical amplifier. *Phys. Rev. B* **2018**, *97*, 241117.
(58) Khanonkin, I.; et al. Room Temperature Quantum Coherent Revival in an Ensemble of Artificial Atoms. *Phys. Rev. Research.* **2021**, *3*, 033073.
(59) Smith, S. J.; Purcell, E. M. Visible Light from Localized Surface Charges Moving Across a Grating. *Phys. Rev.* **1953**, *92*, 1069.
(60) Van den Berg, P. M. Smith-Purcell Radiation from a Point Charge Moving Parallel to a Reflection Grating. *J. Opt. Soc. Am.* **1973**, *63*, 1588.
(61) Tsesses, S.; et al. Light generation via quantum interction of electrons with periodic nanostructures. *Phys. Rev. A* **2017**, *95*, 013832.
(62) Gerry, C.; Knight, P.*Introductory Quantum Optics*; Cambridge University Press, 2004.
(63) Polkovnikov, A. Phase space representation of quantum dynamics. *Ann. Phys.* **2010**, *325*, 1790.
(64) Nazarov, V. U. Multipole surface-plasmon-excitation enhancement in metals. *Phys. Rev. B* **1999**, *59*, 9866.
(65) Nazarov, V. U.; et al. Role of the kinematics of probing electrons in electron energy-loss spectroscopy of solid surfaces. *Phys. Rev. B* **2016**, *93*, 035403.
(66) Nazarov, V. U.; et al. Probing mesoscopic crystals with electrons: One-step simultaneous inelastic and elastic scattering theory. *Phys. Rev. B* **2017**, *96*, 235414.

https://doi.org/10.1021/acs.nanolett.2c03396
Nano Lett. XXXX, XXX, XXX−XXX